Chapter 18

Fourier Analysis for Axisymmetric Boundaries

In this chapter, some axisymmetric numerical tests with the canonical equations shall be described. The idea was to verify the validity of the equations derived, including the method for finding RBM tractions through use of the Riesz theorem, with suitable example cases for which some analytical results were available. Fourier analysis was used in order to further reduce the system sizes, to make computations on ordinary computers feasible, and all the numerical solutions in this section utilized ordinary Gaussian elimination solution of the discrete linear system. The use of the deflate-and-iterate techniques of the preceding chapter will be illustrated in the next chapter, when we consider true three-dimensional geometries.

18.1 How the Components Separate in Wave-Number

Utilizing the axisymmetry of boundaries is easy when the flow is axisymmetric, *e.g.*, due to axial translation or axial rotation. For nonaxisymmetric boundary conditions the problem is somewhat more involved. In elasticity problems efforts have been made by Mayr [49], Rizzo and Shippy [61], Mayr *et al.* [50], and Shippy *et al.* [64], among others. The underlying idea is that on using cylindrical polar coordinates, with the physical components of the fields of interest multiplying the corresponding unit vectors, we may effect a separation of the Fourier components in the azimuthal variable ϕ. This is most easily seen by noting that the differential operators in the equations of interest (here the Stokes equations),

$$\mu \nabla^2 \boldsymbol{v} = \nabla p \tag{18.1}$$

$$\nabla \cdot \boldsymbol{v} = 0 , \tag{18.2}$$

preserve factors of the form $e^{\imath m \phi}$ multiplying functions independent of ϕ; for a collection of formulas, see Bird *et al.* [4, Table A.7-2 in Appendix A]. Obviously a similar method may then be used for any linear differential equation

systems stemming from isotropic physical problems to obtain decoupling of the mentioned Fourier components. What makes this decoupling particularly interesting to us is that all the rigid-body motion velocity fields are expressible in terms of components with wave-numbers $m \in \{0, 1\}$. The term *wave-number* for m is preferred here instead of *frequency*, reserving the latter for time-dependent problems. As a consequence of the above, mobility and resistance problems with axisymmetric boundaries require solving only problems with wave-numbers 0 and 1. Note that the separation of the ϕ-variable from the equations leaves us with two-dimensional arguments, so that reducing the dimensionality further by using the BIE approach will result in a scalar argument, *i.e.*, one gets one-dimensional integral equations. This argument will correspond to the location on a generating curve of the axisymmetric surface. Obviously this reduction can potentially bring large savings in grid generation and computational costs, while enhancing achievable accuracy. A problem on effecting this decomposition is, how to evaluate the elliptic integrals arising in the azimuthal ϕ-integrations. Dealing only with the case of axial translation, Youngren and Acrivos [72] used directly the complete elliptic integrals of the first and second kind. Since then other authors have devised different ways to deal with these in the case of higher wave-numbers, see, *e.g.*, Shippy *et al.* [64] and Hsu and Ganatos [32].

18.2 Another Symmetry Argument for the Fourier Decomposition

In this section we present an elementary symmetry argument in order to clarify why the Fourier decomposition works out the way it does in the case of axisymmetric boundaries. The argument utilizes just the rotational symmetry of the geometry and the linearity and isotropy of the Stokes and continuity equations, without any need for using the actual form of these equations. Thus the same kind of argument can be applied to any problem for which the governing equations are linear and isotropic.

On an axisymmetric surface consider the velocity field given by

$$\boldsymbol{v} = g_\rho(z)\cos(m\phi)\hat{\boldsymbol{e}}_\rho + g_\phi(z)\sin(m\phi)\hat{\boldsymbol{e}}_\phi + g_z(z)\cos(m\phi)\hat{\boldsymbol{e}}_z \ , \tag{18.3}$$

which is its own reflection through the plane $y = 0$. This boundary velocity is assumed to determine the solution in all of the fluid domain considered (recall we have the uniqueness theorem for Stokes flows, and with smooth enough boundary conditions — satisfying mass conservation, *etc.* — we also know the existence of the Stokes solution). Rotation of this velocity surface field by α corresponds to substituting $\phi \leftarrow \phi - \alpha$ in the RHS of the equation above, while everything else there remains unchanged, and produces the velocity field $\boldsymbol{v}_\alpha$. The addition formulas for the trigonometric functions show that for a given fixed $\boldsymbol{v}$, $\boldsymbol{v}_\alpha$ depends linearly on the parameters $\sin(m\alpha)$ and $\cos(m\alpha)$. Since the equations are assumed linear, we infer

Conjecture 1 *If the boundary conditions depend linearly on a set of parameters, so does the whole flow field and the corresponding stress field.*

So the surface tractions $\boldsymbol{T}$ will also depend linearly on the two parameters, "$\cos(m\alpha)$" and "$\sin(m\alpha)$", for example,

$$\hat{\boldsymbol{e}}_\rho(\phi) \cdot \boldsymbol{T}_\alpha(\phi, z) = A(\phi, z)\cos(m\alpha) + B(\phi, z)\sin(m\alpha) \; . \tag{18.4}$$

On the other hand due to the rotational symmetry,

$$\hat{\boldsymbol{e}}_\rho(\phi) \cdot \boldsymbol{T}_\alpha(\phi, z) = \hat{\boldsymbol{e}}_\rho(\phi - \alpha) \cdot \boldsymbol{T}(\phi - \alpha, z) = A(\phi - \alpha, z) \; , \tag{18.5}$$

and so

$$\begin{aligned} A(\phi - \alpha, z) &= A(\phi, z)\cos(m\alpha) + B(\phi, z)\sin(m\alpha) \\ \Rightarrow A(\alpha, z) &= A(0, z)\cos(m\alpha) - B(0, z)\sin(m\alpha) \; . \end{aligned} \tag{18.6}$$

Using this in the expression for the tractions gives

$$\hat{\boldsymbol{e}}_\rho(\phi) \cdot \boldsymbol{T}(\phi, z) = A(\phi, z) = A(0, z)\cos(m\phi) - B(0, z)sin(m\phi) \; . \tag{18.7}$$

Requiring invariance under the reflection about $y = 0$ implies $B(0, z) = 0$, so that

$$\hat{\boldsymbol{e}}_\rho(\phi) \cdot \boldsymbol{T}(\phi, z) = A(0, z)\cos(m\phi) \; . \tag{18.8}$$

Similar treatment of the other components of the surface tractions leads to $\boldsymbol{T}$ being of the same form as $\boldsymbol{v}$, with just the z-dependence modified.

Note that the only assumption needed about the tractions in the deduction above was that the surface field in question must linearly depend on the given boundary conditions. Thus any such surface vector field necessarily has the same form (*i.e.*, the same vectorial Fourier-components) as the velocity and tractions above. In particular, this applies to the double layer density.

18.3 Analytical Fourier Decomposition of the Kernel with Toroidals

Mainly cases where the flow and stress fields are mirror symmetric with respect to the plane $y = 0$ in Cartesian coordinates shall be considered. Then on the surface these fields and the surface tractions have their ϕ-dependence in the form of $\hat{\boldsymbol{e}}_\rho \cos(m\phi)$, $\hat{\boldsymbol{e}}_\phi \sin(m\phi)$, or $\hat{\boldsymbol{e}}_z \cos(m\phi)$. At every point of the surface these are used as a local basis, and after azimuthal integrations an equation system for the ϕ-independent coefficients of these vectors is found. Axial rotation is an exception ($m = 0$ above drops $\hat{\boldsymbol{e}}_\phi$), and one has to consider $\hat{\boldsymbol{e}}_\phi$ alone to get the component of torque along z-axis; clearly $\hat{\boldsymbol{e}}_\phi$ is not mirror symmetric. The remaining two components for $m = 0$ give an equation pair involving F_z. Finally with $m = 1$ the above-mentioned fields correspond to F_x and T_y, so that these have to be solved from an integral equation triplet. Note that the

remaining Fourier components $\hat{e}_\rho \sin(m\phi)$, *etc.* can be reduced to the case above by a rotation of the coordinate axes about z; obviously one then gets F_y and T_x for $m = 1$, so that these need not be considered separately. The following formula, valid for integral m and n,

$$\int_0^{2\pi} \frac{\cos(m\phi)}{q^{n+1/2}}\, d\phi = c_n(k) Q^n_{m-1/2}(k) \;, \tag{18.9}$$

where $q = k - \cos(\phi)$, $k > 1$ and

$$c_n(k) = \frac{(-1)^n 2^{3/2}}{(1/2)_n (k^2-1)^{n/2}} \tag{18.10}$$

$$(1/2)_n = \Gamma(1/2+n)/\Gamma(1/2) \;, \tag{18.11}$$

shows that one type of the elliptic integrals needed can be related to *toroidal functions*, a particular case of associated Legendre functions. Once this has been realized, trigonometric identities and recurrence relations for toroidal functions can be used to similarly relate the rest of the integrals needed to these functions. This gives a systematic method for treating the kernels in any of the integral equations that have been formulated for Stokes flow to get a Fourier decomposition. The analytical work for the double layer kernel was done for all values of the wave-number m simultaneously. It is just the numerical evaluation of these functions that gets more complicated as m is increased. However, as noted, one need not consider other values than $m = 0$ and $m = 1$ for resistance or mobility problems, as long as the configuration of boundaries is axisymmetric.

18.4 Numerical Computation of the Toroidal Functions

Recognizing the elliptic integrals as toroidal functions not only gives us a number of representations, recurrence relations, and asymptotic formulae, but also different algorithms for their computation and tabulated values. Tabulated values and some numerical methods can be found in Briggs and Lowan [8], and backward recursion has been studied by Gautschi [24]. Asymptotic formulae and other properties are available in Gradshteyn and Ryzhik [25] and Magnus and Oberhettinger [47], and in particular Snow [65] contains a wealth of information. A generalization of the arithmetic geometric mean method for complete elliptic integrals, called Bartky's lemma, can be found in Wimp [70], and the algorithm of Fettis [18] is analytically equivalent to this, but numerically easier to implement. The algorithm of Fettis was chosen, with a minor modification. Since the functions computed are singular at argument value one ($k = 1$), the deviation from one ($k - 1$) was used in all the iteration formulae. After this modification the computed values are accurate to double precision over all of the range tested.

In the computations to form the kernel functions, some very small and very large numbers do come up, so that it has been necessary to use the extended

number range provided by g_floating in VAX Fortran. To further enhance accuracy, the computer algebra program MACSYMA[1] was used to factor coefficients in the kernel functions, so that catastrophic cancellation could be avoided. This factoring was also necessary for assessing the behavior of the coefficients near the singularities. Asymptotic analysis reveals, then, that only one of the kernel functions is singular. The diagonal element corresponding to the azimuthal angle ϕ has a logarithmic singularity, whereas all the others remain bounded. This knowledge is essential in performing singularity subtraction with vector functions, where only one component can be cancelled at a time.

18.5 The Numerical Solution Procedure

18.5.1 The Choice of the Numerical Method

The typical method for the solution of BIE systems is to use boundary elements. This means that the surfaces are subdivided into elements over which the solutions are approximated by typically a linear combination of some basis functions, just as in finite element methods, and appropriate quadratures are used for the integrations over elements. In the current case the kernel functions are costly to compute, and therefore it is no longer economical to use a large number of kernel function evaluations for each degree of freedom in the resulting linear system. A method that completely avoids the element aspect is combining a global quadrature with collocation at the quadrature points. In the numerical examples the fact that the integrations are in only one variable makes this choice easy to implement, whereas for two-dimensional surface integrals generating the quadratures in a flexible way could require the use of element approach again. Some quadratures for surface integrals are known though (see Stroud [67]). A difficulty one faces immediately after this choice is how to deal with the singularities at the collocation points. Also for boundary element methods the way that integrations over the singular elements are carried out has a great influence on the accuracy of the results, and even "nearly singular elements" are considered separately. It has been shown that for weakly singular integral equations, the so-called singularity subtraction technique leads to convergent algorithms (Fenyö and Stolle [17]). Using the known outside null functions of the operator, namely densities that coincide with the velocity fields of rigid-body motions on the surface, this technique can be implemented. Power and Miranda had also noticed this possibility, although the singularity subtraction was disguised in the form of an operator identity in connection with their full surface implementation using elements. They utilized the three null functions related to translations, whereas here also those related to rotations are used. Actually with a full surface method one cannot utilize more than three of the null functions for singularity subtraction, but it should be pointed out

[1]MACSYMA was originally developed by the Mathlab Group of the MIT Laboratory of Computer Science, formerly Project MAC, and is currently being enhanced, supported, and distributed by Symbolics, Inc. of Cambridge, Massachusetts. See [68].

that there is some choice. *Also, essential to the success of the singularity subtraction in the codes is that most of the kernel functions are nonsingular.* This observation was facilitated by recognizing the appearance of toroidal harmonics as the elliptic integrals to be calculated, so that the asymptotic behavior of the kernel elements near the singularity could be analyzed. For a general presentation of the various methods for solving integral equations of the second kind see Atkinson [2].

18.5.2 Theory of Singularity Subtraction

Suppose we want to solve an equation of the second kind, $x + Kx = b$, for x. Approximating the integration by a quadrature we get

$$x(s) + \sum_{j=1}^{N} w_j K(s, t_j) x(t_j) = b(s), \tag{18.12}$$

where w_j and t_j $(j = 1, \ldots, N)$ represent the quadrature weights and points, respectively. On using collocation to solve these equations, it is necessary to choose the quadrature points as the collocation points, *i.e.*, to substitute t_i for s above. When the kernel is singular at the collocation point, we cannot evaluate $K(t_j, t_j)$, and this method seems to break down. If, however, we know any nontrivial identity $Kh = g$, this may be subtracted with a suitable multiplier to get

$$x(s)\left(1 + \frac{g(s)}{h(s)}\right) + \int K(s,t)\left(x(t) - \frac{x(s)}{h(s)}h(t)\right) dt = b(s)\ , \tag{18.13}$$

and on discretizing this as above, the function on which the kernel is acting will be zero at the singular point s. Thus the difficulty is avoided. The null functions that are known in the application here were used in exactly the way described to remove singularities. A formal justification for the method can be found in Fenyö and Stolle [17], based on the theory of Kantorovich, for the case where h is identically one. This seems to be the only case usually mentioned (see also Delves and Walsh [13]), probably because the modification here can be easily transformed to this particular case. All one needs to do is to consider h as part of the kernel and to modify the IE correspondingly to

$$\frac{x(s)}{h(s)} + \int \frac{K(s,t)h(t)}{h(s)} \frac{x(t)}{h(t)}\, dt = \frac{b(s)}{h(s)}\ , \tag{18.14}$$

for which the integral identity now reads

$$\int \frac{K(s,t)h(t)}{h(s)}\, dt = \frac{g(s)}{h(s)}\ . \tag{18.15}$$

Naturally it must be required that h is nonzero almost everywhere.

18.6 Axial Torque as an Example

18.6.1 The Azimuthal Integrations

The Fourier analysis and singularity subtraction techniques shall be illustrated here with the simplest case of one integral equation for the axial torque on an axisymmetric particle. As mentioned earlier, axial force leads to two and transverse force and torque to three coupled one-dimensional integral equations, due to the vector nature of Stokes flow problems. Let an axisymmetric surface be generated by the curve $(\rho(t), z(t))$, $t_{min} \le t \le t_{max}$, and consider two surface points (here in cylindrical coordinates) $\boldsymbol{\xi} = (\rho, \phi, z)$ and $\boldsymbol{\eta} = (\tilde{\rho}, \tilde{\phi}, \tilde{z})$ determined by (t, ϕ) and $(\tilde{t}, \tilde{\phi})$. Let the double layer density be $\boldsymbol{\varphi}(\boldsymbol{\xi}) = f(t)\hat{\boldsymbol{e}}_\phi(\phi)$. The goal here is to calculate $\hat{\boldsymbol{e}}_\phi(\tilde{\phi}) \cdot \mathcal{K}\boldsymbol{\varphi}(\boldsymbol{\eta})$. First note that

$$dS = J(t)\, dt\, d\phi \,, \tag{18.16}$$

where

$$J(t) = \rho(t)\sqrt{\rho'(t)^2 + z'(t)^2} \tag{18.17}$$

and the surface normal is

$$\hat{\boldsymbol{n}}(\boldsymbol{\xi}) = a(t)\hat{\boldsymbol{e}}_\rho(\phi) + b(t)\hat{\boldsymbol{e}}_z \,. \tag{18.18}$$

When the generating curve is traversed in the positive (anticlockwise) direction, the coefficients are

$$a = z'/\sqrt{\rho'^2 + z'^2} \tag{18.19}$$

$$b = -\rho'/\sqrt{\rho'^2 + z'^2} \tag{18.20}$$

for the *outward* unit normal. Then

$$\hat{\boldsymbol{e}}_\phi(\tilde{\phi}) \cdot \mathcal{K}\boldsymbol{\varphi}(\boldsymbol{\eta}) = \int_{t_{min}}^{t_{max}} \left\{ \int_0^{2\pi} \hat{\boldsymbol{e}}_\phi(\tilde{\phi}) \cdot \frac{\boldsymbol{rrr} \cdot \hat{\boldsymbol{n}}(\boldsymbol{\xi})}{r^5} \cdot \hat{\boldsymbol{e}}_\phi(\phi)\, d\phi \right\} \frac{3}{2\pi} f(t) J(t)\, dt \,, \tag{18.21}$$

where $\boldsymbol{r} = \boldsymbol{\eta} - \boldsymbol{\xi}$. Consider the inner integrand only. Writing $\boldsymbol{\xi} = \rho\hat{\boldsymbol{e}}_\rho(\phi) + z\hat{\boldsymbol{e}}_z$ with a similar expression for $\boldsymbol{\eta}$ leads to

$$\rho \sin(\Delta\phi)\, [a(\tilde{\rho}\cos(\Delta\phi) - \rho) + b\Delta z]\, \tilde{\rho}\sin(\Delta\phi)/r^5 \,, \tag{18.22}$$

where $\Delta\phi = \tilde{\phi} - \phi$, with similar notation for other cylindrical coordinates. Now

$$r^2 = (\Delta z)^2 + \rho^2 + \tilde{\rho}^2 - 2\rho\tilde{\rho}\cos(\Delta\phi) \,, \tag{18.23}$$

so that $r = l\sqrt{k - \cos(\Delta\phi)}$ with

$$l = l(\tilde{t}, t) = \sqrt{2\rho\tilde{\rho}} \tag{18.24}$$

$$k = k(\tilde{t}, t) = 1 + \left((\Delta z)^2 + (\Delta\rho)^2\right)/(2\rho\tilde{\rho}) > 1 \quad \text{for } \tilde{t} \neq t. \tag{18.25}$$

One can replace $\Delta\phi$ everywhere by ϕ, formally by a suitable substitution followed by a shift of the integration interval (using the 2π periodicity of the integrand). Defining $q = k - \cos(\phi)$ the integrand is now

$$\frac{\rho\tilde{\rho}}{l^5}\frac{[a(\tilde{\rho}\cos(\phi) - \rho) + b\Delta z](1 - \cos^2(\phi))}{q^{5/2}} . \tag{18.26}$$

Substituting $\cos(\phi) = k - q$ in the numerator and expanding it into a polynomial in q gives integrand terms related to toroidal functions with argument k. On denoting the result from the azimuthal integration by $I(\tilde{t}, t)$,

$$\hat{e}_\phi(\tilde{\phi}) \cdot \mathcal{K}(f(t)\hat{e}_\phi)(\eta) = \int_{t_{min}}^{t_{max}} I(\tilde{t}, t)\frac{3}{2\pi}f(t)J(t)\,dt , \tag{18.27}$$

for any $f(t)$. With more calculations of this type, and especially making use of the parity of the integrands, it can be shown that the Fourier components really are separated; specifically $\hat{e}_\phi$-type dependence on $\tilde{\phi}$ is obtained from only the same type of double layer density, as above. This is not surprising, as we know that the mapping of velocity boundary conditions to tractions preserves the Fourier components. On the other hand, the double layer density is just a difference in surface velocities (by the jump condition) found by matching the tractions of the interior and exterior solutions. Another point of view is that the double layer density depends linearly on the velocity boundary conditions, and therefore the symmetry argument given in the beginning of this chapter applies.

18.6.2 Discretizing with Quadrature and Singularity Subtraction

In cylindrical coordinates

$$\begin{aligned} \frac{1}{2}(T_z\hat{e}_z \times \nabla) \cdot \mathcal{G}(\eta) &= \frac{T_z}{8\pi\eta^3}\hat{e}_z \times \left(\tilde{\rho}\hat{e}_\rho(\tilde{\phi}) + \tilde{z}\hat{e}_z\right) \\ &= \frac{T_z\tilde{\rho}}{8\pi\eta^3}\hat{e}_\phi(\tilde{\phi}) . \end{aligned} \tag{18.28}$$

(For convenience we are setting $\mu = 1$ here.) This is the only term from the Stokeslet and rotlet that has the kind of ϕ-dependency considered here. So only T_z comes up as an added variable in this case of a single integral equation, as expected. Considering only the relevant Fourier component of the disturbance surface velocity field, $u(t)\hat{e}_\phi$, the equation is

$$u(\tilde{t}) = f(\tilde{t}) + \int_{t_{min}}^{t_{max}} I(\tilde{t}, t)\frac{3}{2\pi}f(t)J(t)\,dt + T_z\frac{\tilde{\rho}}{8\pi\eta^3} . \tag{18.29}$$

Axial rotation with the angular velocity $\hat{e}_z$ causes the RBM surface velocity field given by

$$\hat{e}_z \times \eta = \tilde{\rho}\hat{e}_\phi(\tilde{\phi}) , \tag{18.30}$$

which is an outside null function. When substituted in place of $f(t)$ above, $\rho(t)$ will cause the f-dependent terms to cancel:

$$0 = \rho(\tilde{t}) + \int_{t_{min}}^{t_{max}} I(\tilde{t},t)\frac{3}{2\pi}\rho(t)J(t)\,dt\ . \tag{18.31}$$

Multiply this equation with $f(\tilde{t})/\rho(\tilde{t})$ and subtract to get

$$u(\tilde{t}) = \int_{t_{min}}^{t_{max}} I(\tilde{t},t)\frac{3}{2\pi}\left[f(t) - \frac{\rho(t)}{\rho(\tilde{t})}f(\tilde{t})\right]J(t)\,dt + T_z\frac{\tilde{\rho}}{8\pi\eta^3}\ . \tag{18.32}$$

Now a quadrature for the interval $[t_{min}, t_{max}]$ can be applied:

$$u(t_i) = \sum_{j\neq i} I(t_i,t_j)\frac{3}{2\pi}\left[f(t_j) - \frac{\rho(t_j)}{\rho(t_i)}f(t_i)\right]J(t_j)w_j + T_z\frac{\rho(t_i)}{8\pi\eta(t_i)^3}\ , \tag{18.33}$$

where w_i and t_i are the quadrature weights and points. To avoid difficulties at the points where the subtracted null function is zero, only such quadratures should be used that do not make use of the endpoints of the interval; for axisymmetric particles with the origin inside, these endpoints will be at the poles on the axis of symmetry. For particles like open toroids, this difficulty does not arise, but then one has to use a circular distribution of Stokeslets or rotlets inside to make use of the Fourier decomposition. To finish the bordering procedure and get a square linear system, one additional orthogonality condition is needed; here the only added variable was T_z. The only RBM density with correct type of ϕ-dependency was already used for singularity subtraction, and the orthogonality condition is

$$\langle f(t)\hat{\mathbf{e}}_\phi, \rho\hat{\mathbf{e}}_\phi\rangle = 0 \tag{18.34}$$

or

$$\oint_S f\rho\,dS = 0\ . \tag{18.35}$$

In discretized form this reads

$$\sum_j w_j f(t_j)\rho(t_j)J(t_j) = 0\ , \tag{18.36}$$

which is the final equation in the discretized system.

To get the surface tractions corresponding to axial rotation with unit angular velocity, denote these by $S(t)\hat{\mathbf{e}}_\phi$. From the Lorentz reciprocal theorem

$$T_z = \langle S(t)\hat{\mathbf{e}}_\phi, u(t)\hat{\mathbf{e}}_\phi\rangle = 2\pi\int_{t_{min}}^{t_{max}} S(t)u(t)J(t)\,dt\ , \tag{18.37}$$

where the 2π came from the ϕ-integration. In discretized form,

$$T_z = 2\pi\sum_j w_j S(t_j)u(t_j)J(t_j)\ . \tag{18.38}$$

The transposing procedure, when applied to the linear system, gives a dependency of the form

$$T_z = \sum_j a_j u(t_j) \ , \tag{18.39}$$

and comparison of the coefficients of $u(t_j)$ implies

$$S(t_j) = \frac{a_j}{2\pi w_j J(t_j)} \ . \tag{18.40}$$

This concludes a fairly complete description of the method applied to a particular Fourier component.

18.7 Transverse Force and Torque

Here are some comments regarding the most complicated case on solving the resistance or mobility problem for axisymmetric surfaces, namely, three coupled one-dimensional IEs involving the transverse force and torque. A less detailed exposition than was given for the case of axial torque shall be given here. The Fourier decomposition of the double layer kernel in terms of toroidal harmonics is given at the end of this section. There are alternative ways of carrying out the Fourier decomposition and discretizing the resulting IEs. For example, it is not necessary to use the toroidal functions when considering only the wave-numbers zero and one, but instead all the integrals involved can be expressed in terms of the ordinary complete elliptic integrals. The advantage of toroidal functions is that all wave-numbers can be handled simultaneously on doing the analytic Fourier decomposition, and the asymptotic properties of the kernel functions can be generally examined.

Restricting our attention to cases mirror symmetric about the Cartesian plane $y = 0$, transverse translation must be parallel to

$$\hat{\boldsymbol{e}}_x = \cos(\tilde{\phi})\hat{\boldsymbol{e}}_\rho(\tilde{\phi}) - \sin(\tilde{\phi})\hat{\boldsymbol{e}}_\phi(\tilde{\phi}) \ . \tag{18.41}$$

Transverse rotation must be about the y-axis, so that this part of the velocity surface field is a multiple of

$$\begin{aligned} \hat{\boldsymbol{e}}_y \times \boldsymbol{\eta} &= \big(\sin(\tilde{\phi})\hat{\boldsymbol{e}}_\rho(\tilde{\phi}) + \cos(\tilde{\phi})\hat{\boldsymbol{e}}_\phi(\tilde{\phi})\big) \times (\tilde{\rho}\hat{\boldsymbol{e}}_\rho(\tilde{\phi}) + \tilde{z}\hat{\boldsymbol{e}}_z) \\ &= \tilde{z}\cos(\tilde{\phi})\hat{\boldsymbol{e}}_\rho(\tilde{\phi}) - \tilde{z}\sin(\tilde{\phi})\hat{\boldsymbol{e}}_\phi(\tilde{\phi}) - \tilde{\rho}\cos(\tilde{\phi})\hat{\boldsymbol{e}}_z \ . \end{aligned} \tag{18.42}$$

It is easy to verify that the Fourier components with this wave-number $m = 1$ and this symmetry are generated by the Stokeslet and rotlet only from $\boldsymbol{F} = F_x\hat{\boldsymbol{e}}_x$ and $\boldsymbol{T} = T_y\hat{\boldsymbol{e}}_y$. That the double layer kernel preserves this type of ϕ-dependency and produces it only from the same type (for axisymmetric surfaces) can be directly verified. Therefore these three vectorial Fourier components allow solving the transverse force and torque in arbitrary flow fields, and by use of the Lorentz reciprocal theorem (in the reversed way) allow finding the surface tractions corresponding to transverse translation or rotation. After separating

the ϕ-dependency from the equations, similar to what was done with the axial torque above, there are three coupled IEs with one-dimensional arguments to be numerically solved. Obviously the RBM velocities for transverse translation and rotation are to be used for singularity subtraction, the integral identities coming from these being null functions as double layer densities. The subtraction was done so that the $\hat{e}_\phi$- and $\hat{e}_z$-components of the unknown density were cancelled at the singular point. To deal with the singularity in the kernel functions, it would be sufficient to just do the first of these cancellations, but it seems to be better to use all the available singularity subtractions to enhance accuracy, even though only one of the kernel functions is singular. The other kernel functions typically have singularities in their derivatives, which causes difficulties in their numerical evaluation; the actual collocation point cannot be used numerically, in any case, since the intermediate results go to infinity, and a nearby point is in large error when the first derivative is unbounded. Finally, the two orthogonality conditions (corresponding to the two added variables) also come from these two null functions, similarly to the case of axial torque.

18.7.1 Fourier Decomposition of the Double Layer Kernel

The following integrals are needed:

$$\mathcal{D}_m^n(k) = \int_0^{2\pi} \frac{\cos(m\phi)}{q^{n+1/2}}\, d\phi = c_n Q_{m-1/2}^n \tag{18.43}$$

$$\begin{aligned}\mathcal{E}_m^n(k) &= \int_0^{2\pi} \frac{\sin^2\phi\cos(m\phi)}{q^{n+1/2}}\, d\phi \\ &= -c_n\sqrt{k^2-1}\left\{kQ_{m-1/2}^{n-1} + \sqrt{k^2-1}(n+m^2-\frac{3}{2})Q_{m-1/2}^{n-2}\right\}\end{aligned} \tag{18.44}$$

$$\mathcal{F}_m^n(k) = \int_0^{2\pi} \frac{\sin\phi\sin(m\phi)}{q^{n+1/2}}\, d\phi = -c_n m\sqrt{k^2-1}Q_{m-1/2}^{n-1}\,. \tag{18.45}$$

The symbols given on the LHSs are introduced for the sake of brevity — they are not standard notation in mathematical literature. Here the argument of every toroidal function is k.

It can be shown that

$$\begin{aligned}\mathcal{K}(\hat{e}_\rho(\phi)\cos(m\phi))(\boldsymbol{\eta}) &= I_{\rho\rho}\hat{e}_\rho(\tilde{\phi})\cos(m\tilde{\phi}) + I_{\phi\rho}\hat{e}_\phi(\tilde{\phi})\sin(m\tilde{\phi}) \\ &\quad + I_{z\rho}\hat{e}_z(\tilde{\phi})\cos(m\tilde{\phi})\,,\end{aligned} \tag{18.46}$$

with similar equations for $\hat{e}_\phi(\phi)\sin(m\phi)$ and $\hat{e}_z\cos(m\phi)$ used as the double layer densities defining the ϕ-independent coefficients $I_{\rho\phi}$, *etc.* These coefficients are listed below in terms of the integrals $\mathcal{D}$, $\mathcal{E}$, and $\mathcal{F}$:

$$\begin{aligned}\frac{2\pi}{3}I_{\rho\rho} = \frac{1}{l^5}\Bigg\{\Bigg[&a\frac{(\tilde{\rho}^2-\rho^2-(\Delta z)^2)(\tilde{\rho}^2-\rho^2+(\Delta z)^2)^2}{8\rho^2\tilde{\rho}} \\ &+b\frac{\Delta z(\tilde{\rho}^2-\rho^2-(\Delta z)^2)(\tilde{\rho}^2-\rho^2+(\Delta z)^2)}{4\rho\tilde{\rho}}\Bigg]\mathcal{D}_m^2\end{aligned}$$

$$+\left[-a\frac{(\tilde{\rho}^2-\rho^2-3(\Delta z)^2)(\tilde{\rho}^2-\rho^2+(\Delta z)^2)}{4\rho}+b(\Delta z)^3\right]\mathcal{D}_m^1$$
$$+\left[-\frac{a}{2}\tilde{\rho}(\tilde{\rho}^2-\rho^2+3(\Delta z)^2)-b\Delta z\rho\tilde{\rho}\right]\mathcal{D}_m^0+\left[a\rho\tilde{\rho}^2\right]\mathcal{D}_m^{-1}\Big\} \quad (18.47)$$

$$\frac{2\pi}{3}I_{\rho\phi} = \frac{-\tilde{\rho}}{l^5}\Big\{\left[a\frac{(\tilde{\rho}^2-\rho^2-(\Delta z)^2)(\tilde{\rho}^2-\rho^2+(\Delta z)^2)}{4\rho\tilde{\rho}}+b\frac{\Delta z(\tilde{\rho}^2-\rho^2-(\Delta z)^2)}{2\tilde{\rho}}\right]\mathcal{F}_m^2$$
$$+\left[a(\Delta z)^2+b\Delta z\rho\right]\mathcal{F}_m^1+\left[-a\rho\tilde{\rho}\right]\mathcal{F}_m^0\Big\} \quad (18.48)$$

$$\frac{2\pi}{3}I_{\rho z} = \frac{\Delta z}{l^5}\Big\{\left[a\frac{(\tilde{\rho}^2-\rho^2-(\Delta z)^2)(\tilde{\rho}^2-\rho^2+(\Delta z)^2)}{4\rho\tilde{\rho}}+b\frac{\Delta z(\tilde{\rho}^2-\rho^2-(\Delta z)^2)}{2\tilde{\rho}}\right]\mathcal{D}_m^2$$
$$+\left[a(\Delta z)^2+b\Delta z\rho\right]\mathcal{D}_m^1+\left[-a\rho\tilde{\rho}\right]\mathcal{D}_m^0\Big\} \quad (18.49)$$

$$\frac{2\pi}{3}I_{\phi\rho} = \frac{\rho}{l^5}\Big\{\left[a\frac{(\tilde{\rho}^2-\rho^2+(\Delta z)^2)^2}{4\rho^2}+b\frac{\Delta z(\tilde{\rho}^2-\rho^2+(\Delta z)^2)}{2\rho}\right]\mathcal{F}_m^2$$
$$+\left[-a\frac{\tilde{\rho}(\tilde{\rho}^2-\rho^2+(\Delta z)^2)}{\rho}-b\Delta z\tilde{\rho}\right]\mathcal{F}_m^1+\left[a\tilde{\rho}^2\right]\mathcal{F}_m^0\Big\} \quad (18.50)$$

$$\frac{2\pi}{3}I_{z\rho} = \frac{\Delta z}{l^5}\Big\{\left[a\frac{(\tilde{\rho}^2-\rho^2+(\Delta z)^2)^2}{4\rho^2}+b\frac{\Delta z(\tilde{\rho}^2-\rho^2+(\Delta z)^2)}{2\rho}\right]\mathcal{D}_m^2$$
$$+\left[-a\frac{\tilde{\rho}(\tilde{\rho}^2-\rho^2+(\Delta z)^2)}{\rho}-b\Delta z\tilde{\rho}\right]\mathcal{D}_m^1+\left[a\tilde{\rho}^2\right]\mathcal{D}_m^0\Big\} \quad (18.51)$$

$$\frac{2\pi}{3}I_{\phi\phi} = \frac{\rho\tilde{\rho}}{l^5}\Big\{\left[a\frac{\tilde{\rho}^2-\rho^2+(\Delta z)^2}{2\rho}+b\Delta z\right]\mathcal{E}_m^2+\left[-a\tilde{\rho}\right]\mathcal{E}_m^1\Big\} \quad (18.52)$$
$$\frac{2\pi}{3}I_{\phi z} = \frac{\rho\Delta z}{l^5}\Big\{\left[a\frac{\tilde{\rho}^2-\rho^2+(\Delta z)^2}{2\rho}+b\Delta z\right]\mathcal{F}_m^2+\left[-a\tilde{\rho}\right]\mathcal{F}_m^1\Big\} \quad (18.53)$$
$$\frac{2\pi}{3}I_{zz} = \frac{(\Delta z)^2}{l^5}\Big\{\left[a\frac{\tilde{\rho}^2-\rho^2+(\Delta z)^2}{2\rho}+b\Delta z\right]\mathcal{D}_m^2+\left[-a\tilde{\rho}\right]\mathcal{D}_m^1\Big\} \quad (18.54)$$
$$I_{z\phi} = -\tilde{\rho}I_{\phi z}/\rho\,. \quad (18.55)$$

The bracketed coefficients in $I_{\rho\phi}$ and $I_{\rho z}$ are the same, with a similar note for the groupings $\{I_{\phi\rho}, I_{z\rho}\}$ and $\{I_{\phi\phi}, I_{\phi z}, I_{z\phi}, I_{zz}\}$.

18.8 Other Details of Implementation

The quadrature chosen was rectangular rule with equal-length subintervals, since the generation of weights is easy and there is great flexibility in choosing the number of quadrature points. On dealing only with axisymmetric particle shapes, little input is required compared with full surface methods. The user needs to give two functions describing the generating curve for the surface in one parameter, $\rho(t)$ and $z(t)$ for $t_{min} \leq t \leq t_{max}$, and two derivatives of these. Similarly, the components of the flow field are given in terms of z and ρ. At first the choice of rectangular quadrature could seem to be restrictive, giving us somehow equidistant points only, but the density of points on the generating curve can easily be modified by using a variable transformation $t = t(\bar{t})$. Viewed differently, the rectangular rule can be used to generate any number of quadratures by changing the integration variable. Still this is not quite as flexible as element methods, but the amount of input remains small, and, after having input the functions, the density of the mesh can be easily changed by just giving one number. *A selection of Fortran programs that illustrate the above ideas are available in the subdirectory, Chapter19, on* "Flossie."

18.9 Limitations of the Fourier Analysis Approach

When the configuration of all of the boundaries involved is nonaxisymmetric, as for a sphere eccentrically inside a cylinder, the different wave-numbers are not decoupled in the equations, since the surface normals do not have a single axis of symmetry. If the Fourier series for the fields are truncated after, say, five wave-numbers, this will lead to a five times bigger linear system than the decoupled wave-numbers individually would give. Depending on the eccentricity of the problem, very high wave-numbers may be significant, so that the Fourier analysis approach has lost its merits. Then it seems more reasonable to go over to a full surface method, where one can implement small surface elements at difficult areas of the surfaces, like those where two surfaces are relatively close together. *Due to the IEs being of the second kind, this will cause no ill-conditioning of the linear system.*

It still remains to be numerically tested if a direct surface quadrature implementation can handle mobility problems with surfaces close together; experience with such problems by related methods suggests that this should be feasible, even though a similar resistance problem would lead to difficulties when the quadrature is not particularly dense around the areas of peaked surface tractions.

18.10 Results from the Axisymmetric Codes

18.10.1 Prolate Spheroids; Comparison of Surface Tractions with Known Analytical Results

The surface tractions on ellipsoids in rigid-body motion in an infinite quiescent fluid are analytically known. In particular, for spheroids the analytical expressions can be formulated in terms of elementary functions, using the results in Brenner [7] and Appendix B of Kim [40]. The same goes for the total force and torque on a spheroid in translation or rotation. A prolate spheroid with axis ratio $b \leq 1$ is generated by

$$\left.\begin{array}{rcl} \rho(t) & = & b\sin(t) \\ z(t) & = & -\cos(t) \end{array}\right\}, \quad \text{for } 0 \leq t \leq \pi. \tag{18.56}$$

Using this parametrization with the chosen quadrature gives points equidistant in the polar angle t of spheroidal polar coordinates. This seems to work a little better than using points equidistant in z. All the programs used (except that for a particle in a container) have been tested with spheroids to verify correctness of the method used and the programming. Here the dependence of the convergence on the number of collocation points with the aspect ratio $1/b$ as parameter, for the case of transverse translation, is presented in Figure 18.1. A comparison of the analytical surface tractions with the numerically found ones in a particular case is shown in Figure 18.2. Of the three cases for the resistance problem with Fourier decomposition, the largest equation system is related to transverse force and torque. With 80 points the number of equations is about 240, and a MicroVAX II requires about 83 seconds of CPU time to solve the problem, including computation of the related RBM tractions. For the two other cases with smaller linear systems, the CPU times are correspondingly shorter, and typically the accuracy achieved is somewhat better with the same mesh. Double precision is used in the computations, and specifically the computation of toroidal functions is always carried out to this precision. In this sense the programs are not optimized; instead of analyzing round-off errors and allowing inaccuracies, these have been avoided as much as possible.

18.10.2 Mesh Effects: Grooved Particles

As a fairly difficult test particle, a sphere with a groove along its equator was chosen. This was generated by using $b = 1$ for the spheroid above and modifying the radial coordinate ρ by subtracting from it a Gaussian type bell shape:

$$\rho(t) = \sin(t) - \alpha \exp[-\frac{(t - \pi/2)^2}{2\beta^2}]. \tag{18.57}$$

In this way there will be no sharp edges on the surface; arbitrary order derivatives of the generating curve are continuous.

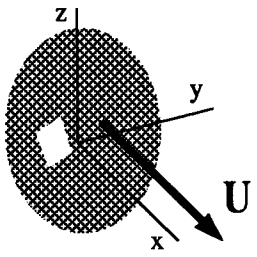

Figure 18.1: Transverse translation of a prolate spheroid.

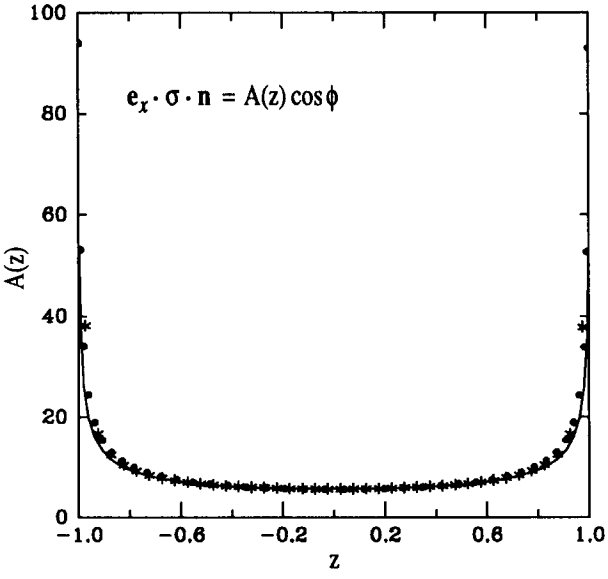

Figure 18.2: The surface tractions on a prolate spheroid (aspect ratio 10).

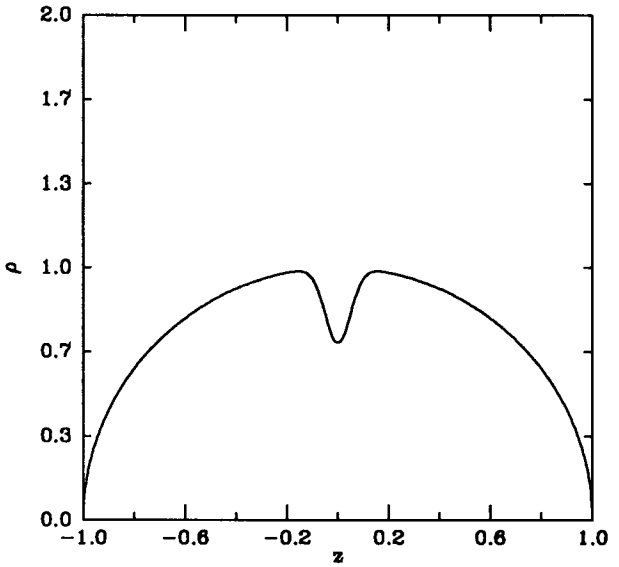

Figure 18.3: The profile of the grooved particle.

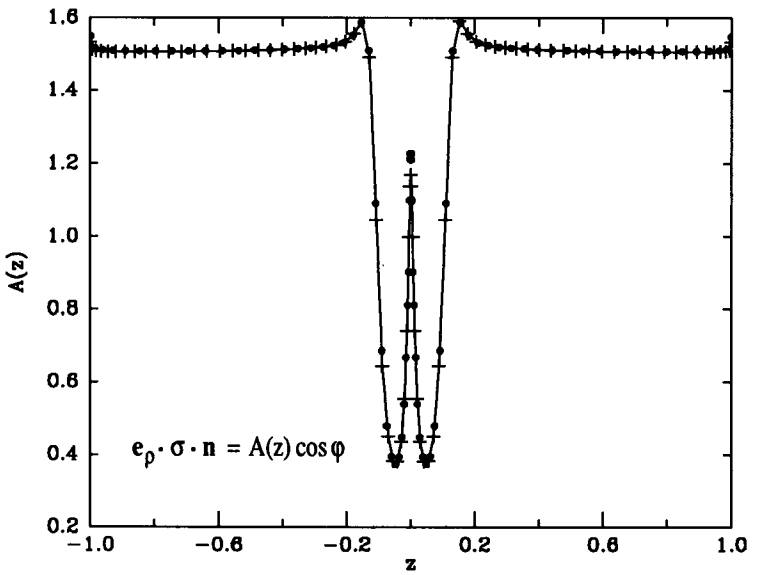

Figure 18.4: The surface tractions on the grooved particle.

In the numerical computations presented here, $\alpha = 0.3$ and $\beta = 0.05$. The resulting profile of the grooved sphere is shown in Figure 18.3. The convergence with this parametrization and the chosen quadrature was slow, so that it was decided to modify the mesh to be more dense around the equator by the following transformations. A "cubic density" is achieved by

$$t = \frac{(\bar{t} - \pi/2)^3}{(\pi/2)^2} + \pi/2, \tag{18.58}$$

and a less pronounced "quadratic density" by

$$t = \frac{(\bar{t} - \pi/2)|\bar{t} - \pi/2|}{\pi/2} + \pi/2. \tag{18.59}$$

These modifications to the parametrization of the generating curve were done in the corresponding subroutine, so that now the quadrature points are equidistant in $\bar{t}$. Use of these gives almost identical results, although the extremely high density at the equator given by the former causes slight difficulties with the surface tractions; see Figure 18.4. This can be understood since pointwise traction values with extremely small weight in the inner product used with the Lorentz reciprocal theorem do not have much effect on the total force or torque; small deviations in them are numerically allowed. It should be noted that use of these distributions of collocation points would lead to severe ill-conditioning with almost any other kind of formulation than IEs of the second kind. Here we are saved by the point evaluation of the unknown function ("the delta function added to the kernel") that distinguishes equations of the second kind from those of the first kind.

18.10.3 The Effect of Sharp Edges: Finite Circular Cylinder

It is well known that sharp corners or edges protruding into the fluid can produce singular surface tractions. One way to analytically assess the behavior of these singularities is by utilizing the Papkovich–Neuber representation in terms of harmonic functions for which the behavior near edges is known (Jaswon and Symm [33]). Chan *et al.* [9] directly transformed the problem of axial rotation to a potential problem, following the method of Jeffery [34], so they did not refer to the representation mentioned above. The numerical computations for the straight circular cylinder show that the edges can be neglected, as long as we are not explicitly interested in the type of singularity at them. The total torque on the cylinder converges fine, and getting about three-digit accuracy requires only 80 points when the cylinder has axis ratio 1 (diameter equals height). The fore-aft symmetry of the cylinder was not utilized, and the parametrization was

$$(\rho, z) = \begin{cases} (t, -1) & \text{for } t \in [0, 1] \\ (1, t-2) & \text{for } t \in [1, 3] \\ (4-t, 1) & \text{for } t \in [3, 4]. \end{cases} \tag{18.60}$$

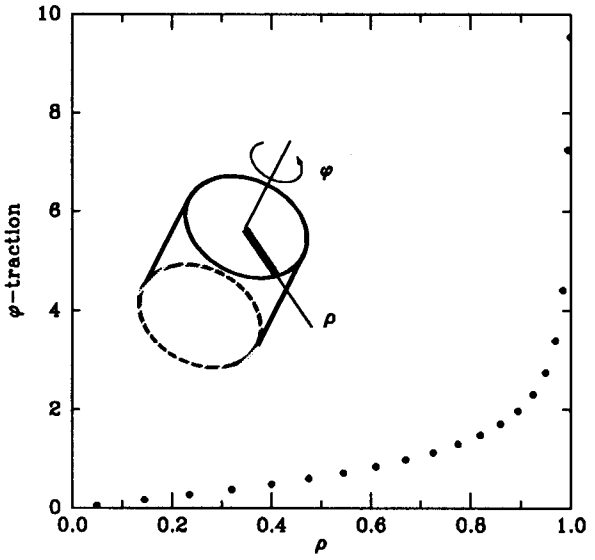

Figure 18.5: The tractions on the "lid" of a rotating cylinder.

With 80 points $T_z = 39.734$, and Chan *et al.* give 39.869. To see if better accuracy is achieved by modifying the mesh, the following "double quadratic modification" was used to get high density at both edges:

$$t = \begin{cases} (\bar{t}-1)|\bar{t}-1|+1 & \text{for } \bar{t} \in [0,2] \\ (\bar{t}-3)|\bar{t}-3|+3 & \text{for } \bar{t} \in [2,4]. \end{cases} \tag{18.61}$$

After this the torque 39.854 is found with 80 points, and the results for surface tractions are plotted along the generating curve on the top of the surface in Figure 18.5. To assess the accuracy of these the same curve was scaled so that the singularity at the edge is cancelled, and plotted also including point values of the tractions given by Chan *et al.* for comparison (see Figure 18.6). The agreement is strikingly good, except for the last two quadrature points closest to the edge, and even these are not in error by much. It is understandable that the quadrature collocation method can be somewhat confused by the presence of an edge, since it nowhere is given information about the exact location of the edge; only information at the collocation points is being used.

The theory of the IEs used was based on the assumption of Lyapunov-smooth surfaces for the reason that then $\hat{\boldsymbol{r}}\cdot\hat{\boldsymbol{n}}/r^{1+\alpha} \to 0$ $(\alpha > 0)$ as $r \to 0$, and this makes the double layer kernel only weakly singular. With edges or corners present, this does not hold any more. The numerical experiment here indicates that no severe difficulties need arise from the presence of edges, although the tractions will (in general) be singular. In practice concentrating more quadrature points

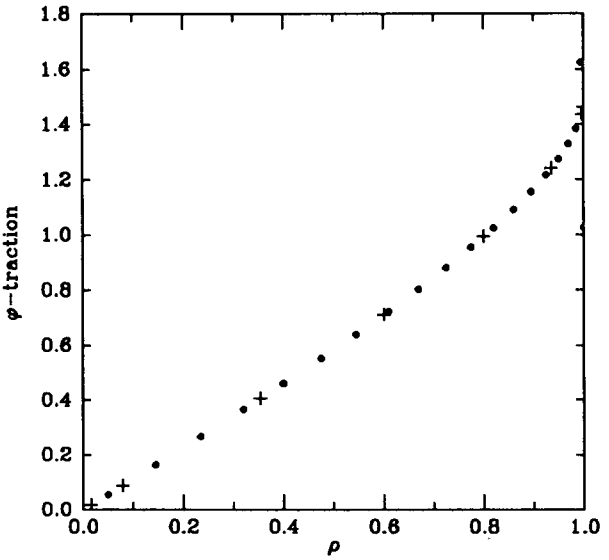

Figure 18.6: Tractions with singularity removed (factored).

where the tractions are large will help in dealing with any numerical difficulties. This is because the quadrature weights will become small and distribute large tractions to a large number of components in the discrete approximation, so it will no longer have large elements. This procedure also allows us to numerically observe the severity of the traction singularity. Similar considerations apply to multisurface problems that are close to lubrication problems, where the local tractions are almost singular. This is essentially the numerical analogue of local stretching of the surface coordinate system about the singular point(s), which could be used analytically in asymptotic analysis. With other general numerically applied formulations, not carrying out the asymptotic analysis separately, such stretching would lead to ill-conditioning caused by too close collocation points.

Finally, the inclusion monotonicity of resistance for Stokes flows noted by Hill and Power [30] — although it has been verified only for smooth surface shapes — suggests strongly that corners and edges may be rounded inwards and outwards to get corresponding bounds for the resistance. Therefore problems with corners may be avoided also by this means if it becomes necessary. Another implication of the inclusion monotonicity is that resistance problems are well-posed relative to surface shape data, meaning that small deviations in particle shape will generally produce only small deviations in resistance when one of the shapes can be bound inside and outside by the other suitably shrunk or expanded. The local surface tractions, however, are not equally well behaved, as

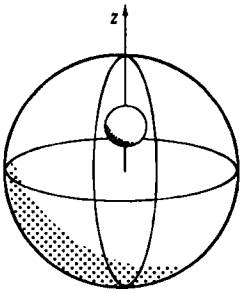

Figure 18.7: A sphere in a spherical container.

can be seen by approximating a smooth surface by a jagged one. For this reason the method introduced is superior to others, since the density of collocation points can be made high in the vicinity of areas of interest without causing catastrophic ill-conditioning. This type of behavior can only be expected of IEs of the second kind.

18.10.4 A Container Problem

A suitable model problem for testing the canonical equations with Fourier decomposition is that of a spherical particle concentrically in a spherical container. In general, the container null function is not explicitly known, and therefore it cannot be used for singularity subtraction; the outside null functions for the container can, however, be used again to get integral identities. The main difference between a container and a particle surface, in this respect, is just the direction in which the surface normal used in the double layer kernel is pointed.

Analytical results, obtained with stream functions are given in Happel and Brenner [29, p.133]. Choosing the container radius to be 1.25 times that of the particle corresponds to $\lambda = 0.8$ in the notation of the reference above (see Figure 18.7), and for this case the reference gives 138.224 as the factor by which the resistance for translation is increased relative to that in unbounded fluid. As the factor indicates, there is a very strong interaction at such a small separation. In this sense the chosen test case is fairly difficult.

The computations were carried out with equal numbers of points on the particle and the container, these being 40, 60, and 80. Using points equidistant in the axial z-coordinate gives the factors 306.4, 160.7, and 146.4. Discretization equidistant in the polar angle seems more reasonable, emphasizing more the polar areas. This gives the much better results 149.7, 143.0, and 140.8, with the same numbers of quadrature points.

This example again illustrates the importance of the choice of the parametrization. Even a bad choice will eventually give results with the desired accuracy as the mesh is refined, but a good choice can save a lot in terms of the problem

Points	equistant-z	equidistant-θ
40	306.4	149.7
60	160.7	143.0
80	146.4	140.8

Table 18.1: Drag on a sphere settling in a spherical container (exact: 138.224).

size and required CPU time. This example also verifies that the canonical equations are correctly formulated for problems with a container.

As discussed earlier, due to the symmetric shape of a sphere, the double layer operator on it is self-adjoint. From this it follows that the container null function on a sphere is actually a multiple of the surface normal, since this is the null function of the adjoint single layer problem. The same result can be seen from the fact that the container null function must remain unchanged by any rotation, since these would by symmetry also give null functions and the null space is one-dimensional. Therefore in this case using the container surface normal to remove the container null function happens to be an even better choice than it usually would be.

18.11 Possibilities for Improvement and Generalization

In the calculations with prolate spheroids, it is noted that the numerical solution becomes more difficult as the shape is more elongated. It seems that this is not so much due to the high curvature of the surface near the poles, since the method easily handles high curvature in other test cases. It is suggested that the reason for added difficulties here is just the lack of distributing the singularities inside the particle, instead of concentrating them on the centroid only. Another possible reason is the way in which the singularity subtraction is carried out, with functions some of which use the radial coordinate ρ. Distributing the singularities inside the particles corresponds to choosing a "more robust" set of basis functions to span the deficient part of the range of the double layer operator. The easiest way to implement a distribution would be to have an *a priori* fixed distribution of Stokeslets (rotlets) that gets multiplied by the total force (torque). A more sophisticated approach would automatically determine the distribution from a solution with a coarse mesh. For oblate particles, preserving axisymmetry would require the use of ring distributions of singularities. These modifications have not been tested so far.

One way to find a suitable distribution of singularities could be the method of Dabros [12]; for a more advanced adaptive variation of the method, see Han and Olson [28]. The approximate solution from this method can then be improved

upon with the bordered equations. This two-stage "predictor-corrector" method can be necessary if one wants to handle difficult shapes or to inspect traction singularities or near-singularities. Current investigations in this direction have yielded promising results.

Exercises

Exercise 18.1 Computer Algebra.
The program package MACSYMA was mentioned in connection with the analytical transformations done before programming. Find out about the availability of computer algebra programs and what they are capable of.

Exercise 18.2 Nyström Method.
The Nyström method of interpolation can be used when solving second-kind IE:s with quadrature collocation. In fact, using quadrature collocation is often called *solution by Nyström's method.* The basic idea is that after discretizing with quadrature, one continuous variable remains in the (approximate) equation. By a small rearrangement this approximate equation provides a "natural" interpolation formula by which values of $x(s)$ can be found once the values $x(t_i)$ are known. With singular kernels this kind of interpolation does not sound too good any more. Check if you can figure out how singularity subtraction could help to some extent. For a good treatment of Nyström's method with continuous kernels, see the book by Atkinson [2].

Exercise 18.3 Traction Singularities.
Try to give a verbal explanation for the tractions being singular at the edges of the rotating cylinder. Similarly, try to explain the traction profile computed for the grooved sphere. Find out the exact analytical corresponding traction profile for a sphere without a groove, and draw it in the same picture for comparison.